HHS Public Access

Author manuscript

J Acoust Soc Am. Author manuscript; available in PMC 2021 June 21.

Published in final edited form as:

J Acoust Soc Am. 1999 December ; 106(6): 3659–3664. doi:10.1121/1.428218.

Frequency dependence of ultrasonic backscatter from human trabecular bone: theory and experiment

Keith A. Wear

U.S. Food and Drug Administration, Center for Devices and Radiological Health, HFZ-142, 12720 Twinbrook Parkway, Rockville, MD 20852

Abstract

A model describing the frequency dependence of backscatter coefficient from trabecular bone is presented. Scattering is assumed to originate from the surfaces of trabeculae, which are modeled as long thin cylinders with radii small compared with the ultrasonic wavelength. Experimental ultrasonic measurements at 500 kHz, 1 MHz, and 2.25 MHz from a wire target and from trabecular bone samples from human calcaneus *in vitro* are reported. In both cases, measurements are in good agreement with theory. For mediolateral insonification of calcaneus at low frequencies, including the typical diagnostic range (near 500 kHz), backscatter coefficient is proportional to frequency cubed. At higher frequencies, the frequency response flattens out. The data also suggest that at diagnostic frequencies, multiple scattering effects on the average are relatively small for the samples investigated. Finally, at diagnostic frequencies, the data suggest that absorption is likely to be a larger component of attenuation than scattering.

Keywords

calcaneus; bone; backscatter; osteoporosis

Introduction

Osteoporosis is a major public health issue. In the United States, over 1.5 million fractures attributed to osteoporosis occur each year. These include fractures in vertebrae (500,000), hip (250,000), and distal forearm (240,000) with annual treatment-related cost exceeding $10,000,000,000[1].

Bone mineral density (BMD) is one of the primary predictive risk factors for osteoporotic fracture[2–7]. An expert panel of the World Health Organization (WHO) has proposed diagnostic criteria for osteoporosis based on BMD measurements. The WHO criteria were recently applied to femoral BMD measured by dual energy x-ray absorptiometry (DEXA) in men and women participating in the third National Health and Nutrition Examination Survey (NHANES III), 1988–1994[5]. The prevalence of osteoporosis (defined by WHO as BMD below a threshold equal to 2.5 standard deviations below the mean of young normal nonHispanic Caucasian women, a threshold intentionally chosen so that the prevalence

kaw@cdrh.fda.gov.

would approximate that of lifetime osteoporotic fractures in Caucasian women) in the USA is 13–18% or 13–17 million[5].

Common methods for assessing bone density include DEXA and quantitative computed tomography (QCT). These methods are expensive, involve ionizing radiation, and require relatively sophisticated equipment and are often unavailable in smaller hospitals with low caseloads. Finally, while these measurements correlate relatively well with bone mineral *density*, they are not necessarily very sensitive to *micro-architecture* or to the protein matrix of bone (which are also important determinants of fracture risk).

Approaches based on ultrasound offer advantages including low cost, lack of ionizing radiation, speed, simplicity, and portability. Most current methods are based on broadband ultrasonic attenuation (BUA) and speed-of-sound (SOS) measurements in the calcaneus. It has been demonstrated that ultrasonic attenuation is highly correlated with calcaneal mass density.[8–11] Calcaneal ultrasonic measurements (BUA combined with SOS) have been shown to perform well for prediction of hip fractures in elderly women in prospective[12,13] and retrospective[14–16] studies. Despite this diagnostic utility, the fundamental mechanisms underlying the interaction between ultrasound and calcaneus are not well understood presently.

Measurements of ultrasonic backscattering properties may provide additional useful information. The decreased number and size of trabeculae (which may serve as scattering sites) within bone that accompany the aging process would be expected to reduce backscatter. The clinical feasibility and diagnostic promise of this measurement have already been demonstrated.[17–19]

The objective of this paper is to investigate mechanisms underlying ultrasonic scattering in trabecular bone. Toward this end, a theoretical model for ultrasonic scattering from trabecular bone is presented and subsequently tested experimentally. Tests are performed to assess the magnitude of multiple scattering effects in trabecular bone.

Theory

Bone tissue may be classified into two types: cortical (or compact) bone and trabecular (or spongy) bone. Cortical bone is most abundant in the shafts of long bones such as the tibia, though it constitutes the outer shell of every bone in the body. Trabecular bone is concentrated in the vertebrae, pelvis, calcaneus, and at the ends of long bones, though it is present in the interiors of all bones. The calcaneus is predominantly composed of trabecular bone covered by a thin cortical shell. Trabecular bone consists of a three dimensional lattice of branching spicules or plates. The spaces between the trabeculae are filled with marrow, which consists of fat and cellular components of blood constituents. In this paper, scattering from trabecular bone is investigated.

Trabeculae within bone are postulated to be the principle sources of ultrasound scattering and are modeled here as cylinders with diameters that are small relative to the ultrasonic wavelength. In addition, it is assumed that these cylinders are long relative to the ultrasound beam cross-section and are oriented perpendicular to the ultrasound propagation direction.

Figure 1 shows the presence of long thin trabeculae within the interior of a calcaneus which is consistent with this model. Although the trabeculae exhibit a myriad of orientations, they are all approximately perpendicular to the ultrasound propagation direction provided that the bone is interrogated in the mediolateral (or lateromedial) direction (perpendicular to the plane of Figure 1). A typical value for human calcaneal trabecular thickness is 120 ± 10 μm (mean ± standard deviation).[20] The wavelengths of ultrasound (in water) used in the experiment were much larger and ranged from 3.1 mm (at 500 kHz) to 0.7 mm (at 2.25 MHz).

The intensity of an acoustic wave scattered from a solid cylinder, I_s, is given by[21,22]

$$I_s = \frac{Ia}{\pi r}|\varphi_s(\phi)|^2 \tag{1}$$

where I is the intensity of the incident plane wave, a is the radius of the cylinder, r is the distance from the cylinder axis to the observation point, and

$$|\varphi_s(\phi)|^2 = \frac{1}{ka}\sum_{m=0}^{\infty}\sum_{n=0}^{\infty}\varepsilon_m\varepsilon_n \sin\eta_m \sin\eta_n \cos(\eta_m-\eta_n)\cos(m\phi)\cos(n\phi) \tag{2}$$

where ϕ is the angle between the incident and observation directions, k = 2π/λ, λ is the wavelength in the fluid surrounding the scatterer, $\varepsilon_0 = 1$, $\varepsilon_m = 2$ (m > 0), η_m is the phase angle for scattering from a cylinder given by[21]

$$\tan\eta_n = \tan\delta_n(x)\frac{\tan\Phi_n + \tan\alpha_n(x)}{\tan\Phi_n + \tan\beta_n(x)} \tag{3}$$

where x = ka,

$$\delta_n(x) = \tan^{-1}[-J_n(x)/N_n(x)], \tag{4}$$

$$\alpha_n(x) = \tan^{-1}[-xJ_n'(x)/J_n(x)], \tag{5}$$

$$\beta_n(x) = \tan^{-1}[-xN_n'(x)/N_n(x)], \tag{6}$$

and

$$\tan\Phi_n = (-\rho/\rho_1)\tan\zeta_n(x_1,\sigma), \tag{7}$$

where, J_m and N_m correspond to Bessel and Neumann functions, primes denote differentiation, ρ is the density of the fluid surrounding the scatterer, ρ_1 is the density of the cylindrical scatterer, and σ = Poisson's ratio. For inelastic scattering, $\tan\Phi_n = 0$ for all n. In general, the scattering phase angle, $\zeta_n(x_1, \sigma)$ is given by

$$\tan\zeta_n(x_1,\sigma) = -\frac{x_2^2}{2}\frac{\dfrac{\tan\alpha_n(x_1)}{\tan\alpha_n(x_1)+1} - \dfrac{n^2}{\tan\alpha_n(x_2)+n^2-x_2^2/2}}{\dfrac{\tan\alpha_n(x_1)+n^2-x_2^2/2}{\tan\alpha_n(x_1)+1} - \dfrac{n^2[\tan\alpha_n(x_2)+1]}{\tan\alpha_n(x_2)+n^2-x_2^2/2}} \quad (8)$$

where $x_1 = k_1a$, $x_2 = k_2a$, $k_1 = \omega/c_1$, $k_2 = \omega/c_2$, c_1 = the compressional wave velocity in the scatterer, and c_2 = the shear wave velocity in the scatterer. Since the ratio of x_1 to x_2 is completely determined by σ, ζ_n may be expressed simply as a function of x_1 and σ. For backscatter, $\phi = 180°$.

Scattered intensities for both inelastic (solid line) and elastic (dashed line) scattering from a cylinder as functions of ka are shown in Figure 2. For the elastic case, material properties for hydroxyapatite (c_1 = 6790 m/s, ρ = 3.22 g/cm^3, and σ = 0.28)[23,24] scatterers in water (c_1 = 1480 m/s at 20°C and ρ = 1.00 g/cm^3) were assumed. Submicroscopic deposits of calcium phosphate, similar but not necessarily identical to hydroxyapatite, $Ca_{10}(PO_4)_6(OH)_2$, are the major inorganic constituents of bone.[25] Anderson, Soo, and Trahey, in modeling microcalcifications in the breast, performed a similar comparison in which they employed inelastic and elastic models for spherical scatterers composed of hydroxyapatite.[24] The relationship between inelastic and elastic scattered intensities are very similar for the two different shapes. For both cylinders and spheres, there are four roughly equally spaced maxima in the range $0 < ka < 5$. The locations of the maxima are approximately the same for the elastic and inelastic cases. For both cylinders and spheres, the first elastic peak is lower in magnitude than the first inelastic peak, while the second through fourth elastic peaks are higher in magnitude.

In the low frequency limit ($ka << 1$), it may be shown that the intensity of the inelastically scattered wave is given by[22]

$$I_s \cong \frac{\pi k^3 a^4}{8r} I(1-2\cos\phi)^2 . \quad (9)$$

Thus, in the low frequency limit, inelastic scattering becomes proportional to the cube of the ultrasonic frequency at all angles. This is at least approximately true for the elastic case, as can be seen in Figure 3, where cubic fits agree well with scattered wave intensities at various angles. The angular distribution of scattering at 500 kHz is illustrated in Figure 4. Scattering is most prominent in the backward direction.

This theory applies to a single cylindrical scatterer. It can also describe the frequency dependence of scattering from a superposition of scattered signals from many cylindrical sources provided two conditions are satisfied. The first condition is that echoes from different sources add incoherently. This will occur if the cylindrical scatterers are positioned sufficiently randomly that the phases of their scattered waves may be taken to be uniformly distributed on the interval from 0 to 2π.[26,27] The second condition is that the effects of multiple scattering are negligible.

Experimental Methods

Biological Methods

Sixteen human (gender and age unknown) calcaneus samples were obtained. They were defatted using a trichloro-ethylene solution. Defatting was presumed not to significantly affect measurements since attenuation[11,28] and speed of sound[28,29] of defatted trabecular bone have been measured to be only slightly different from their counterparts with marrow left intact. The cortical lateral sides were sliced off leaving two parallel surfaces with direct access to trabecular bone. The thicknesses of the samples varied from 14 to 21 mm. In order to remove air bubbles, the samples were vacuum degassed underwater in a desiccator. After vacuum, samples were allowed to thermally equilibrate to room temperature prior to ultrasonic interrogation. Ultrasonic measurements were performed in distilled water at room temperature. The temperature was measured for each experiment and ranged between 19.1 °C and 21.2 °C. The relative orientation between the ultrasound beam and the calcanei was the same as with *in vivo* measurements performed with commercial bone sonometers, in which sound propagates in the mediolateral (or lateromedial) direction.

Apparent density, the ratio of the dehydrated, defatted tissue mass to the total specimen volume,[11] was measured for each sample. Mass was measured using a balance. Volume was assessed from separate measurements of thickness and cross-sectional area. Thickness between the two parallel planar surfaces (cut by machine) was measured using calipers. Cross-sectional areas were measured by computer processing of scanned images of the samples.

Ultrasonic Methods

In addition to the bone samples, a wire oriented perpendicular to the ultrasound propagation direction was interrogated. These measurements were used to validate the measurement methodology and the numerical computation for the frequency-dependent backscatter from a cylinder (Equation 2 with ϕ=180°). Repeated measurements were performed in order to generate means and standard deviations.

A Panametrics (Waltham, MA) 5800 pulser/receiver was used. Samples were interrogated in a water tank using Panametrics circular, focussed, broadband transducers with center frequencies of 500 kHz, 1 MHz, and 2.25 MHz. Received ultrasound signals were digitized (8 bit, 10 MHz) using a LeCroy (Chestnut Ridge, NY) 9310C Dual 400 MHz oscilloscope and stored on computer (via GPIB) for off-line analysis.

Backscatter coefficients were measured using a reference phantom method.[30] With this method, the dependences of measurements on machine-dependent factors (e.g. transducer aperture, distance from transducer to sample, transducer electromechanical response, gain settings, etc.) are minimized. A reference phantom with known frequency-dependent backscatter coefficient, $\eta_R(f)$, and attenuation coefficient, $\alpha_R(f)$, placed in the water tank at the same distance as for the bone samples was used. The phantom consisted of glass spheres in agar with $\alpha_R(f)=0.124f^{1.63}$ dB/cm, c = 1556 m/s, $\eta_R(f)=1.15\times10^{-4}$, 1.46×10^{-3}, and 9.35×10^{-3} $cm^{-1}Sr^{-1}$ at 500 kHz, 1 MHz, and 2.25 MHz respectively. Power spectra from the

bone samples, $I_B(f)$, and the phantom $I_R(f)$ were acquired. The backscatter coefficient, $\eta_B(f)$, is then obtained from

$$\eta_B(f) = \frac{1}{T^4}\frac{G[\alpha_B(f), l]}{G[\alpha_R(f), l]}\frac{I_B(f)}{I_R(f)}\eta_R(f) \quad (10)$$

where T is the amplitude transmission coefficient at the water/bone interface. Due to the high degree of porosity of the samples, T was assumed to be one.[31] The function G[α(f), l] compensates for attenuation effects and is given by[26]

$$G[\alpha(f), l] = \frac{4\alpha(f)l}{1 - e^{-4\alpha(f)l}} \quad (11)$$

where l is the gate length. Good agreement between experimental measurements using this method and theoretical predictions based on Faran's theory of scattering from spheres[21] for ultrasonic backscatter coefficients from phantoms has been previously reported by this laboratory.[32] (Note that Equation 11 differs from a previously used attenuation compensation function[19] since in the present experiment there was water rather than tissue or phantom between the transducer and the gated volume).

Attenuation measurements were required in order to compensate signals prior to backscatter coefficient estimation. Attenuation was measured using a standard through-transmission method. Using two opposing coaxially-aligned transducers (one transmitter and one receiver), transmitted signals were recorded both with and without the bone sample in the acoustic path. The bone samples were larger in cross-sectional area than the receiving transducer apertures. Attenuation coefficient was then estimated using a log spectral difference technique.[33] In principle, this substitution technique can exhibit appreciable error if the speed of sound differs substantially between the sample and the reference.[34] However, one study indicates that this diffraction-related error is negligible in the calcaneus.[31] Evidently the speed of sound in the calcaneus, approximately 1475 – 1650 m/s[31], is sufficiently close to that of distilled water at room temperature, 1487 m/s,[35] that diffraction-related errors may be ignored.

Results

The means and standard deviations for the measured properties of the calcaneus samples were 0.33 ± 0.11 g/ml (apparent density), 9.94 ± 5.74 dB/cmMHz (attenuation slope), and 0.062 ± 0.066 $cm^{-1}Sr^{-1}$ (backscatter coefficient at 500 kHz).

Figure 5 shows experimental measurements of backscatter coefficient for the wire target. Also shown are the general frequency dependent inelastic backscatter (Equation 1 with ϕ=180°) and the low frequency cubic approximation (Equation 9 with ϕ=180°) based on the actual radius of the wire (a = 191 μm). The magnitudes of the theoretical curves were arbitrarily adjusted to fit the data. Good agreement in frequency dependence between theory and experiment may be seen.

Figure 6 shows experimental measurements of average backscatter coefficient for the 16 calcaneus samples. Also shown are the general frequency dependent backscatter (Equation 1 with ϕ=180°) for both the inelastic model (solid line) and the elastic model (dashed line) as well as the low frequency cubic approximation (Equation 9 with ϕ=180°) assuming the material properties for hydroxyapatite given above and a = 60 μm.[20] Again, the magnitudes of the theoretical curves were arbitrarily adjusted to fit the data. There is little difference in the frequency dependences for the inelastic and elastic models in the low frequency range examined here. Good agreement in frequency dependence between both theoretical models and experiment may be seen. The low frequency data (300 – 700 kHz) were least squares fit to power law functions, Af^n, where A is an arbitrary multiplicative constant and n is the exponent. For the 16 samples, n was found to be 3.26 ± 0.20 (mean ± standard error), very close to the expected cubic dependence.

Figure 7 shows frequency dependent experimental measurements for backscatter coefficients for the bone samples, now divided into two subgroups: the 8 lowest density and the 8 highest density. Both subgroups exhibit essentially the same frequency dependence. The high-density group backscatters more strongly in a uniform fashion throughout the set of frequencies employed. The means and standard errors of ratios of high-to-low backscatter coefficients were comparable for all three transducer center frequencies: 2.4 ± 0.6 (500 kHz data), 2.5 ± 0.3 (1 MHz data), and 2.3 ± 0.3 (2.25 MHz data).

Discussion

A model describing the frequency dependence of backscatter coefficient from trabecular bone has been presented. Scattering was assumed to originate from the surfaces of trabeculae, which were modeled as long thin cylinders with radii small compared with the ultrasonic wavelength. Experimental ultrasonic measurements at 500 kHz, 1 MHz, and 2.25 MHz from a wire target and from trabecular bone samples from human calcaneus *in vitro* have been presented. In both cases, measurements were in good agreement with theoretical predictions. For insonification in the mediolateral direction at low frequencies ($ka << 1$), including the typical diagnostic range (near 500 kHz), backscatter coefficient is proportional to frequency cubed. At higher frequencies, the frequency response flattens out.

The data presented here have implications with regard to the relative roles of scattering and absorption in determining attenuation in trabecular bone at diagnostic frequencies. Attenuation in the range between 300 kHz and 700 kHz has been found in numerous studies to be approximately proportional to frequency to the first power.[8–11] The theoretical model presented here predicts that, at low frequencies, scattering in all directions is approximately proportional to frequency cubed. These two different frequency dependences could be consistent if absorption is a larger component of attenuation than scattering.

The data presented here suggest that, at typical diagnostic frequencies (near 500 kHz), the effects of multiple scattering on the average are relatively small for the samples investigated. This is evidenced in Figure 6 as, in the low frequency regime, the theoretically expected frequency cubed dependence of backscatter coefficient was observed. Multiple scattering, if present, would have had the effect of applying additional high pass (frequency cubed)

filtering to the echoes (via multiple scatters), resulting in a measured backscatter coefficient with a more rapid than cubic frequency dependence. Even if multiple scattering were present, the relatively high attenuation coefficient of trabecular bone would tend to suppress it as multiply scattered waves tend to traverse longer path lengths than singly scattered waves.

Measurements of the frequency dependence of scattering might in principle be used to infer scatterer size (here trabecular width), similar to methodology successfully employed by Insana and co-workers to evaluate sizes of different scattering components in kidney.[36–38] However, several factors would make accurate, diagnostically-useful determination of trabecular width extremely challenging. First, the size of the calcaneus is rather small, limiting the quantity of data that can be averaged for backscatter coefficient estimation. Second, the high attenuation coefficient of calcaneus limits the bandwidth of frequencies available for analysis.

Figure 7 illustrates the potential diagnostic utility of the backscatter coefficient measurement. That is, higher backscatter coefficients are associated with denser bones. This result reinforces a previously published finding in normal individuals *in vivo* in which a measure of the magnitude of ultrasonic backscatter was found to correlate highly with bone density assessed using QCT.[19]

Acknowledgements

The author is grateful for funding provided by the US Food and Drug Administration Office of Women's Health. In addition, the suggestions of Matthew Myers, FDA, and William Sacks, FDA, are greatly appreciated.

References

1. Lenchik L and Sartoris DJ. Current concepts in osteoporosis, Amer. J. Roent 168, 905–911 (1997).
2. Melton LJ et al., Long-term fracture prediction by bone mineral assessed at different skeletal sites, J. Bone Miner. Res 8, 1227–1233, (1993). [PubMed: 8256660]
3. Black DM DM et al., Axial and appendicular bone density predict fracture in older women. J Bone Miner. Res 7, 633–638, (1992). [PubMed: 1414481]
4. Cummings SR SR et al. The study of osteoporotic fractures research group: Bone density at various sites for the prediction of hip fractures. Lancet 341, 72–75, (1993). [PubMed: 8093403]
5. Looker AC et al. Prevalence of low femoral bone density in older U.S. adults from NHANES III. J Bone Miner. Res 12, 1761–1768, (1997). [PubMed: 9383679]
6. Kanis JL et al. The diagnosis of osteoporosis. J Bone Miner. Res 9, 1137–1141, (1994). [PubMed: 7976495]
7. World Health Organization. Assessment of fracture risk and its application to screening for postmenopausal osteoporosis. Technical Report Series No 843 WHO, Geneva, Switzerland.
8. Langton CM, Palmer SB, and Porter RW. The measurement of broadband ultrasonic attenuation in cancellous bone, Eng. in Med 13, 89–91, (1984). [PubMed: 6540216]
9. Rossman P, Zagzebski J, Mesina C, Sorenson J, and Mazess R, Comparison of Speed of Sound and Ultrasound Attenuation in the Os Calcis to Bone Density of the Radius, Femur and Lumbar Spine, Clin. Phys. Physiol.Meas, 1989; 10:353–360. [PubMed: 2698780]
10. Tavakoli MB and Evans JA. Dependence of the velocity and attenuation of ultrasound in bone on the mineral content. Phys. Med. Biol, 36, 1529–1537, (1991). [PubMed: 1754623]
11. Langton CM, et al., Prediction of Mechanical Properties of the Human Calcaneus by Broadband Ultrasonic Attenuation, Bone, 18, 495–503, (1996). [PubMed: 8805988]

12. Hans D et al., Ultrasonographic heel measurements to predict hip fracture in elderly women: the EPIDOS prospective study, Lancet, 348, 511–514, (1996). [PubMed: 8757153]
13. Bauer DC et al. Broadband ultrasound attenuation predicts fractures strongly and independently of densitometry in older women, Arch. Intern, Med 157, 629–634 (1997). [PubMed: 9080917]
14. Schott M et al., Ultrasound discriminates patients with hip fracture equally well as dual energy X-ray absorptiometry and independently of bone mineral density. J. Bone Min. Res, 10, 243–249 (1995).
15. Turner CH et al. Calcaneal ultrasonic measurements discriminate hip fracture independently of bone mass, Osteo. International, 5, 130–135 (1995).
16. Glüer CC et al. Osteoporosis: Association of recent fractures with quantitative US findings, Radiology, 199, 725–732 (1996). [PubMed: 8637996]
17. Wear KA and Garra BS. Assessment of bone density using broadband ultrasonic backscatter, Proc. 22nd Int. Symp Ultrason. Imag. and Tissue Char, Washington, DC. 1997; 14 (Abstract).
18. Giat P, Chappard C, Roux C, Laugier P, and Berger G. Preliminary clinical assessment of the backscatter coefficient in osteoporosis, Proc. 22nd Int. Symp Ultrason. Imag. and Tissue Char, Washington, DC, 1997, 16 (Abstract).
19. Wear KA and Garra BS. Assessment of bone density using ultrasonic backscatter. Ultrason. Med. & Biol 24, 689–695, (1998).
20. Hausler KD, Rich PA, Smith PC, Barry EB. Relationships between static histomorphometry and ultrasound in the human calcaneus. Calcif. Tissue. Int 64:477–480, (1999). [PubMed: 10341018]
21. Faran JJ, Sound scattering by solid cylinders and spheres, J. Acoust. Soc. Am, 23, 405–418 (1951)
22. Morse PM and Ingard KU, Theoretical Acoustics Princeton, NJ, Princeton University Press, 1986.
23. Grenoble DE, et al., The elastic properties of hard tissues and apatites, J. Biomed. Mater. Res, 6, 221–233, 1972. [PubMed: 5027322]
24. Anderson ME, Soo MSC, and Trahey GE, Microcalcifications as elastic scatterers under ultrasound, IEEE Trans. Ultrason., Ferro., Freq. Cont 45, 925–934.
25. Heany RP, “Calcium,” in Principles of Bone Biology, edited by Bilezikian JP, Raisz LG, and Rodan Gideon A., (Academic Press, San Diego, 1996).
26. O’Donnell M and Miller JG, Quantitative broadband ultrasonic backscatter: An approach to nondestructive evaluation in acoustically inhomogeneous materials, J. Appl. Phys 52, 1056–1065 (1981)
27. Madsen EL, Insana MF, and Zagzebski JA. Method of data reduction for accurate determination of acoustic backscatter coefficients, J. Acoust. Soc. Am, 76, 913–923, (1984). [PubMed: 6491053]
28. Alves JM, Ryaby JT, Kaufman JJ, Magee PP, and Siffert RS. Influence of marrow on ultrasounic velocity and attenuation in bovine trabecular bone. Calc. Tissue. Int, 58, 362–367, (1996).
29. Njeh CF and Langton CM. The effect of cortical endplates on ultrasound velocity through the calcaneus: an *in vitro* study. Brit. J. Radiol, 70, 504–510, (1997). [PubMed: 9227233]
30. Zagzebski JA, Yao LX, Boote EJ, and Lu ZF, “Quantitative Backscatter Imaging,” in Ultrasonic Scattering in Biological Tissues, edited by Shung KK and Thieme GA, (CRC Press, Boca Raton, FL, 1993).
31. Droin P, Berger G, and Laugier P. Velocity dispersion of acoustic waves in cancellous bone. IEEE Trans. Ultrason. Ferro. Freq. Cont 45, 581–592 (1998)
32. Wear KA, Garra BS, and Hall TJ, Measurements of ultrasonic backscatter coefficients in human liver and kidney *in vivo*, J. Acoust. Soc. Am, 98, 1852–1857 (1995) [PubMed: 7593911]
33. Kuc R and Schwartz M. Estimating the acoustic attenuation coefficient slope for liver from reflected ultrasound signals. IEEE Trans. Son. Ultrason SU-26, 353–362, (1979).
34. Xu W and Kaufman JJ. Diffraction correction methods for insertion ultrasound attenuation estimation. IEEE Trans. Biomed. Eng 40, 563–570, (1993). [PubMed: 8262538]
35. Pierce AD, Acoustics: An Introduction to Its Physical Principles and Applications (McGraw-Hill, New York, 1981), p. 31.
36. Insana MF and Brown DG, “Acoustic scattering theory applied to soft biological tissues,” in Ultrasonic Scattering in Biological Tissues, edited by Shung KK and Thieme GA, (CRC Press, Boca Raton, FL, 1993).

37. Insana MF, Hall TJ, and Fishback JL. Identifying acoustic scattering sources in normal renal parenchyma from the anisotropy in acoustic properties. Ultrason. Med. Biol, 17, 613–626, (1991).

38. Hall TJ, Insana MF, Harrison LA, and Cox GG. Ultrasonic measurement of glomerular diameters in normal adult humans. Ultrason. Med. Biol, 22, 987–997, (1996).

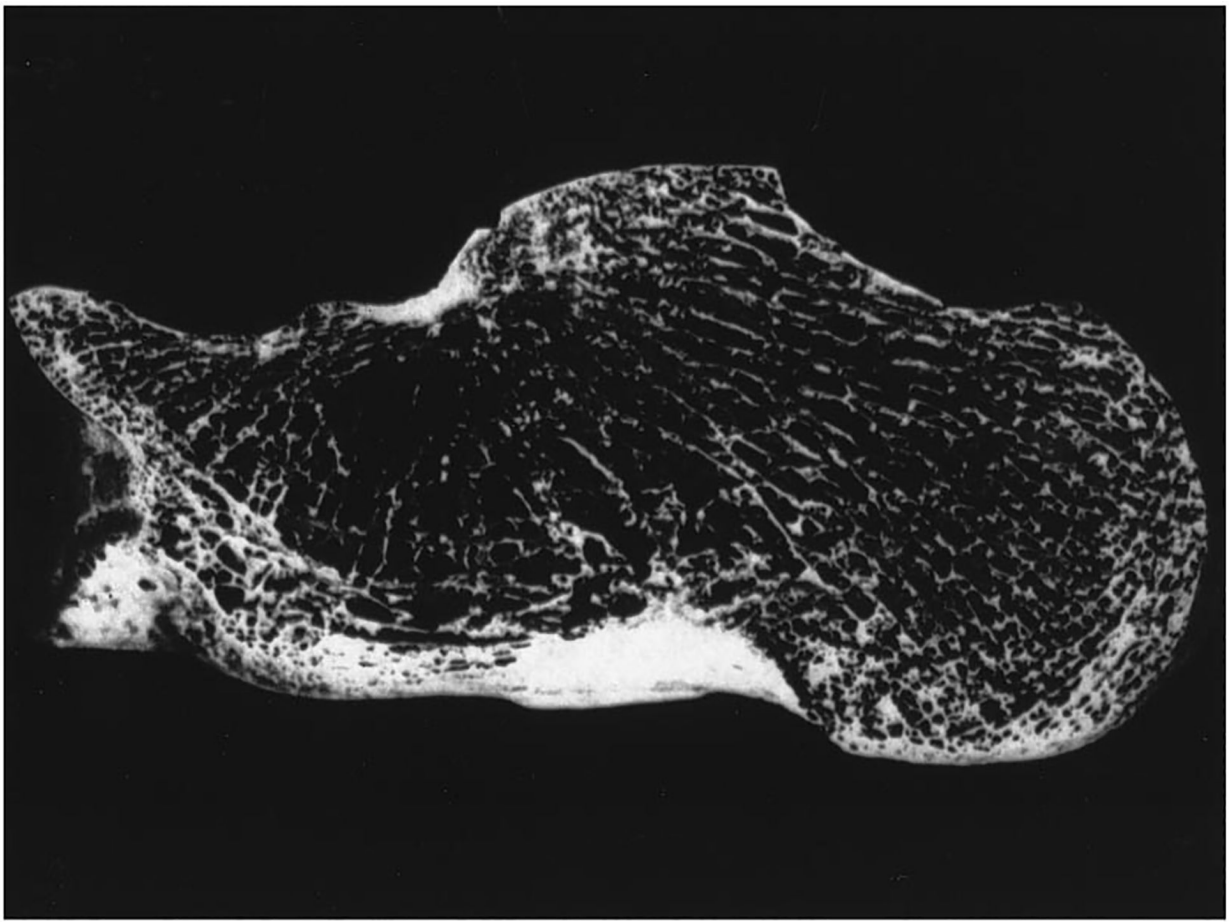

Figure 1.
Calcaneus sample with lateral cortical layers removed. Long thin trabeculae are apparent.

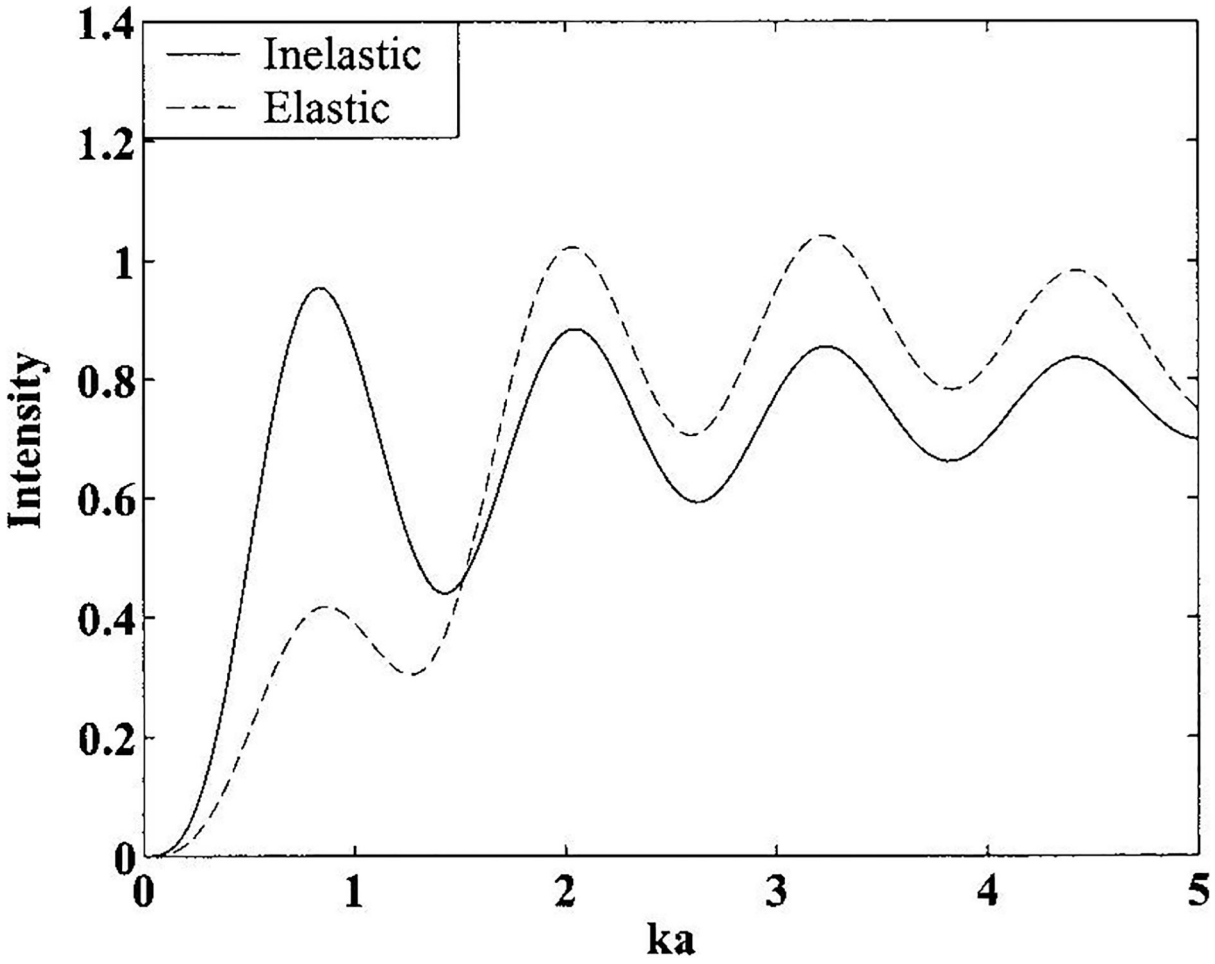

Figure 2.

Theoretical backscatter from a hydroxyapatite cylinder immersed in water as a function of ka where $k = 2\pi/\lambda$ and a is the radius. The solid curve corresponds to the inelastic model and the dashed curve corresponds to the elastic model.

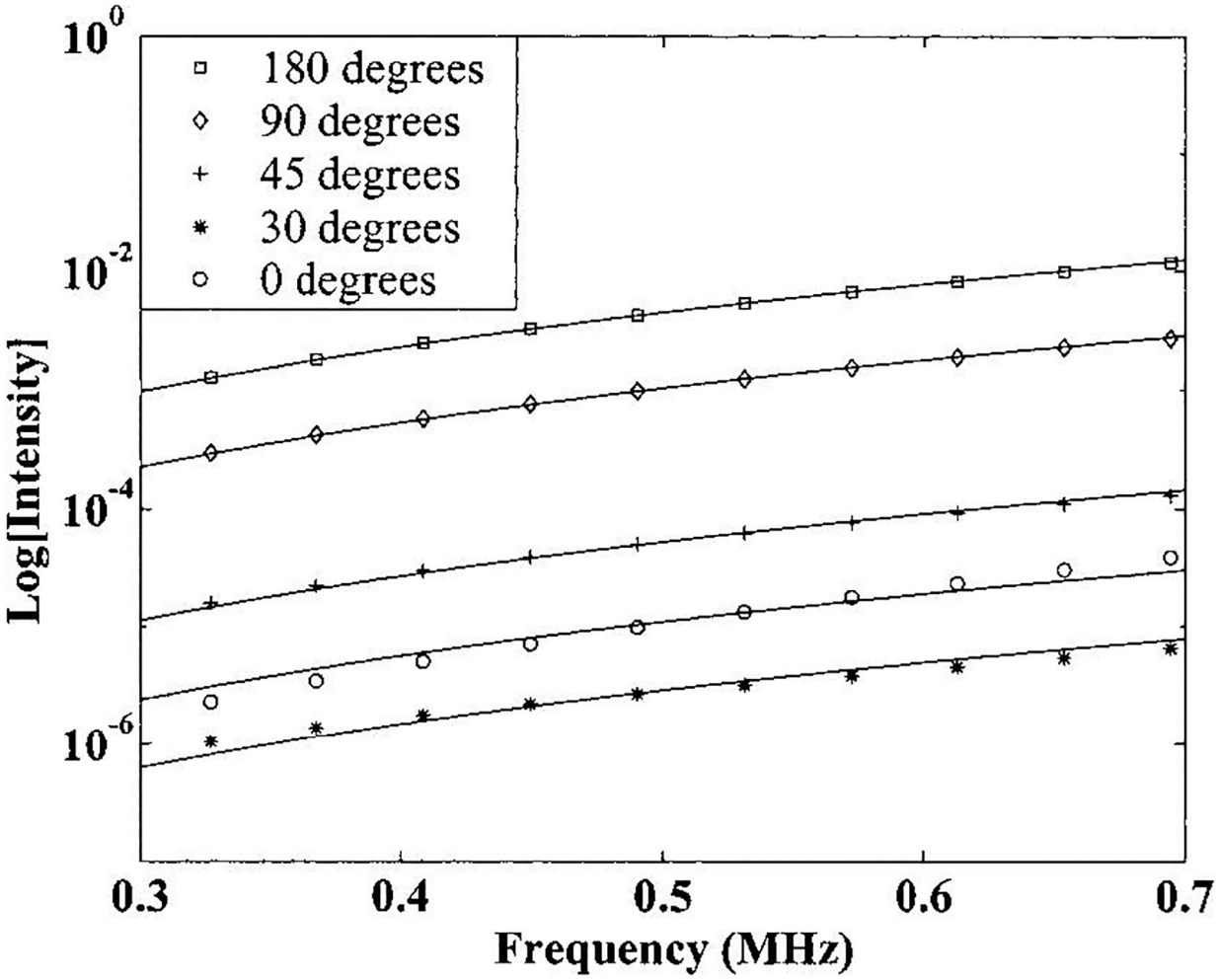

Figure 3.

The logarithm of the intensity of an elastically scattered wave from a hydroxyapatite cylinder vs. frequency for various angles (ϕ). Also shown are cubic fits to the data. The apparent juxtaposition of the 0° and 30° data is due to minima in the angular distribution at ±25°.

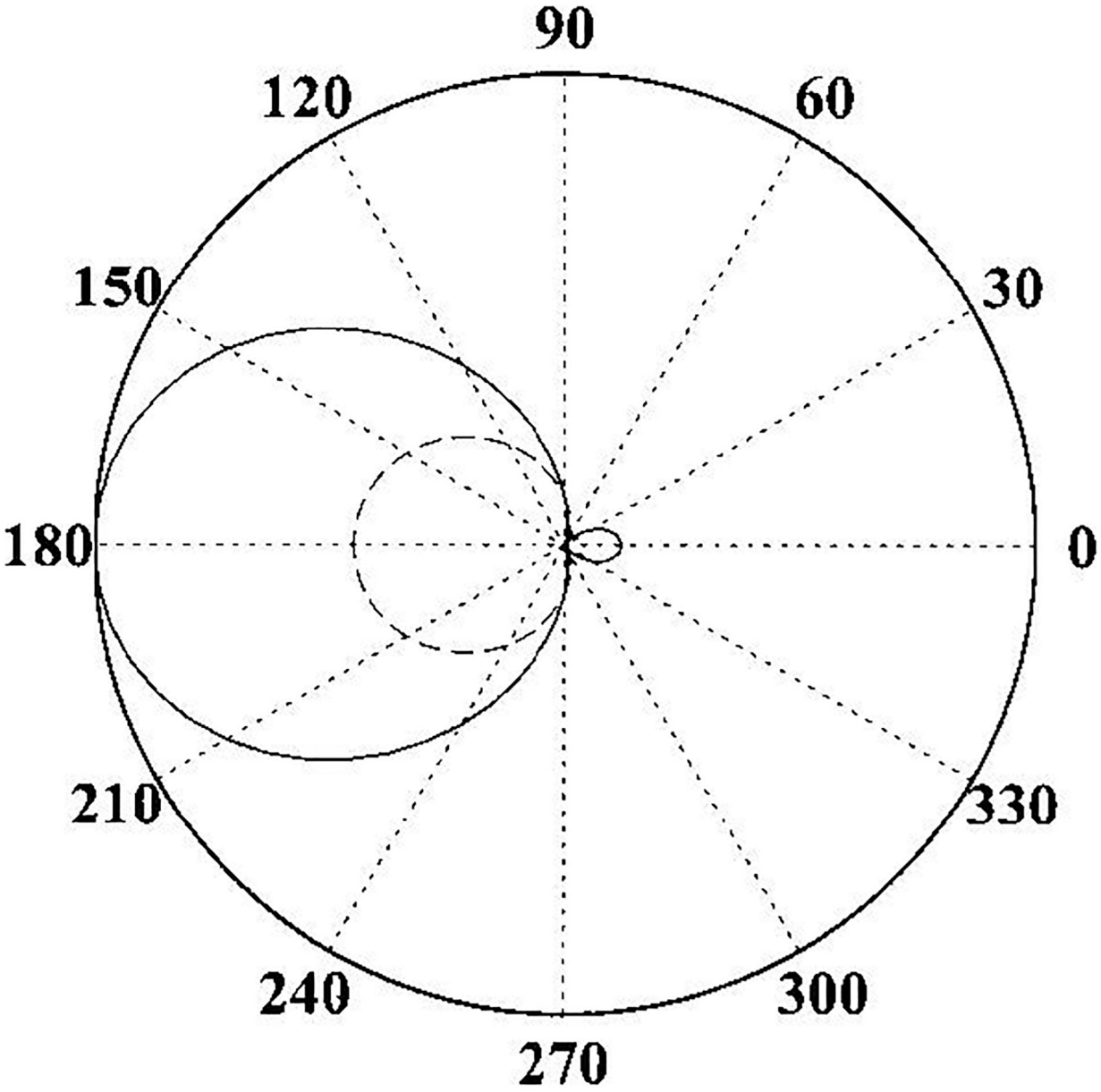

Figure 4.
Angular distribution of scattering for the inelastic case (solid line) and elastic case (dashed line). Scattering is most prominent in the backward direction.

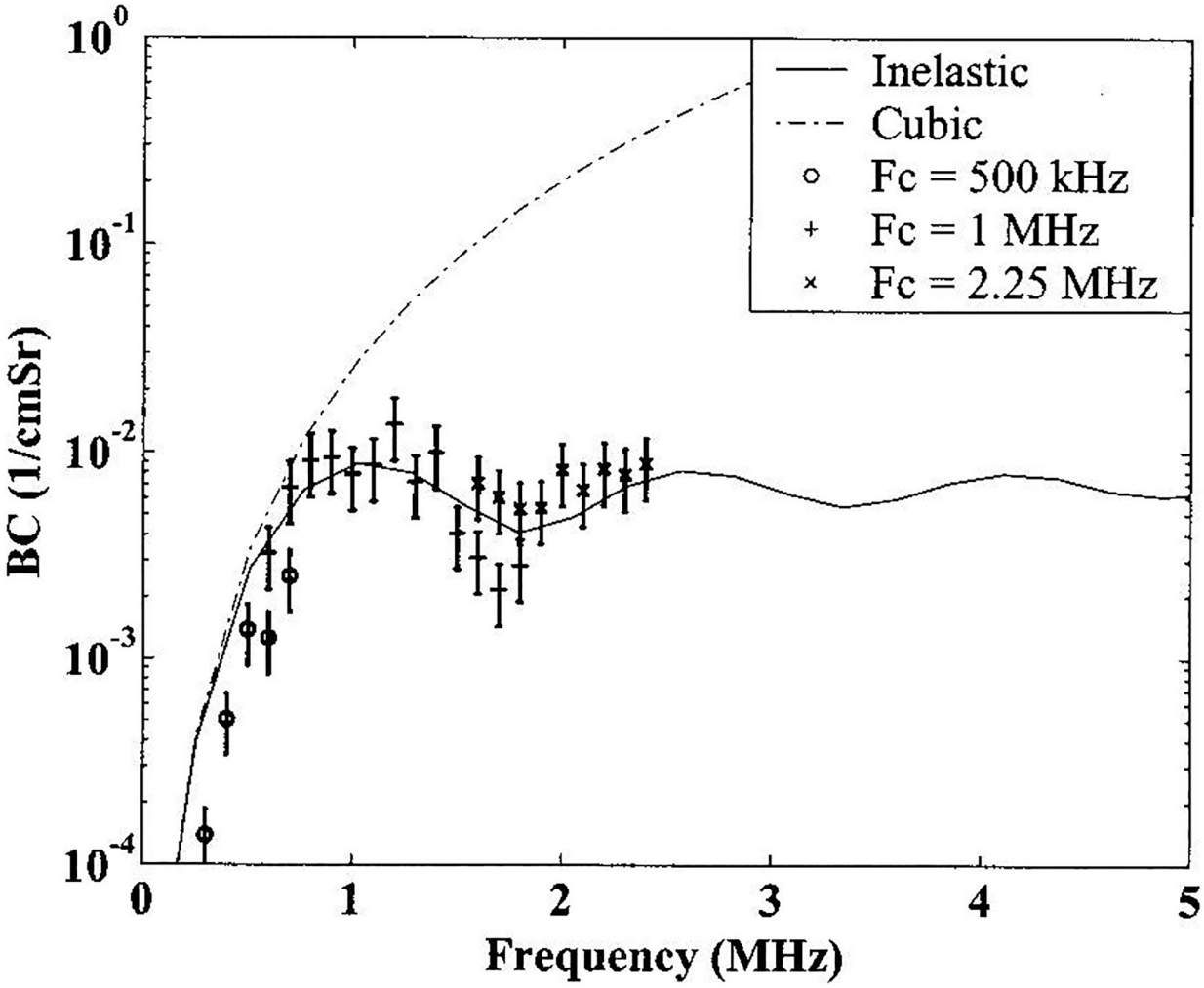

Figure 5.

Backscatter from a wire test object. The solid curve is the theoretical frequency-dependent backscatter from a rigid cylinder (Equation 1 with ϕ=180°) based on the actual radius of the wire (a = 191 μm). The chain-dashed curve is the low frequency cubic approximation (Equation 9 with ϕ=180°). The magnitudes of the theoretical curves were arbitrarily selected to fit the data. Good agreement in frequency dependence between theory and experiment may be seen. Error bars denote standard errors of measurements. The three symbols correspond the center frequencies of the three transducers used: 500 kHz (circle), 1 MHz (+), and 2.25 MHz (x).

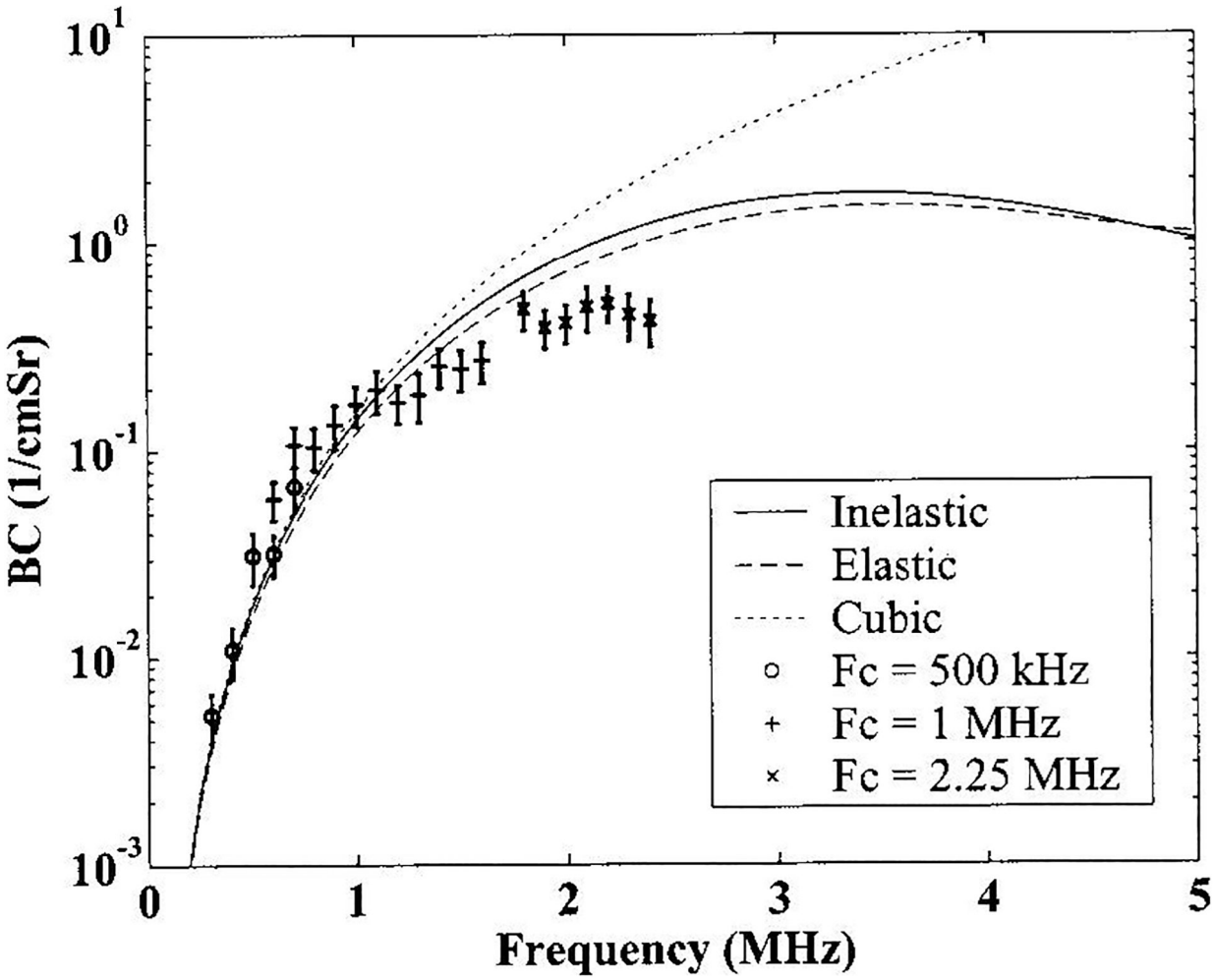

Figure 6.

Experimental measurements of average backscatter coefficient for the 16 calcaneus samples. Also shown are the inelastic (solid line) and elastic (dashed line) frequency dependent backscatter coefficients (Equation 1 with ϕ=180°) based on a published value for the average radius of calcaneal trabeculae. The dotted line is the low frequency cubic approximation (Equation 9 with ϕ=180°). Again, the magnitudes of the theoretical curves were arbitrarily selected to fit the data. Good agreement in frequency dependence between theory and experiment may be seen. Error bars denote standard errors of measurements. The three symbols correspond the center frequencies of the three transducers used: 500 kHz (circle), 1 MHz (+), and 2.25 MHz (x).

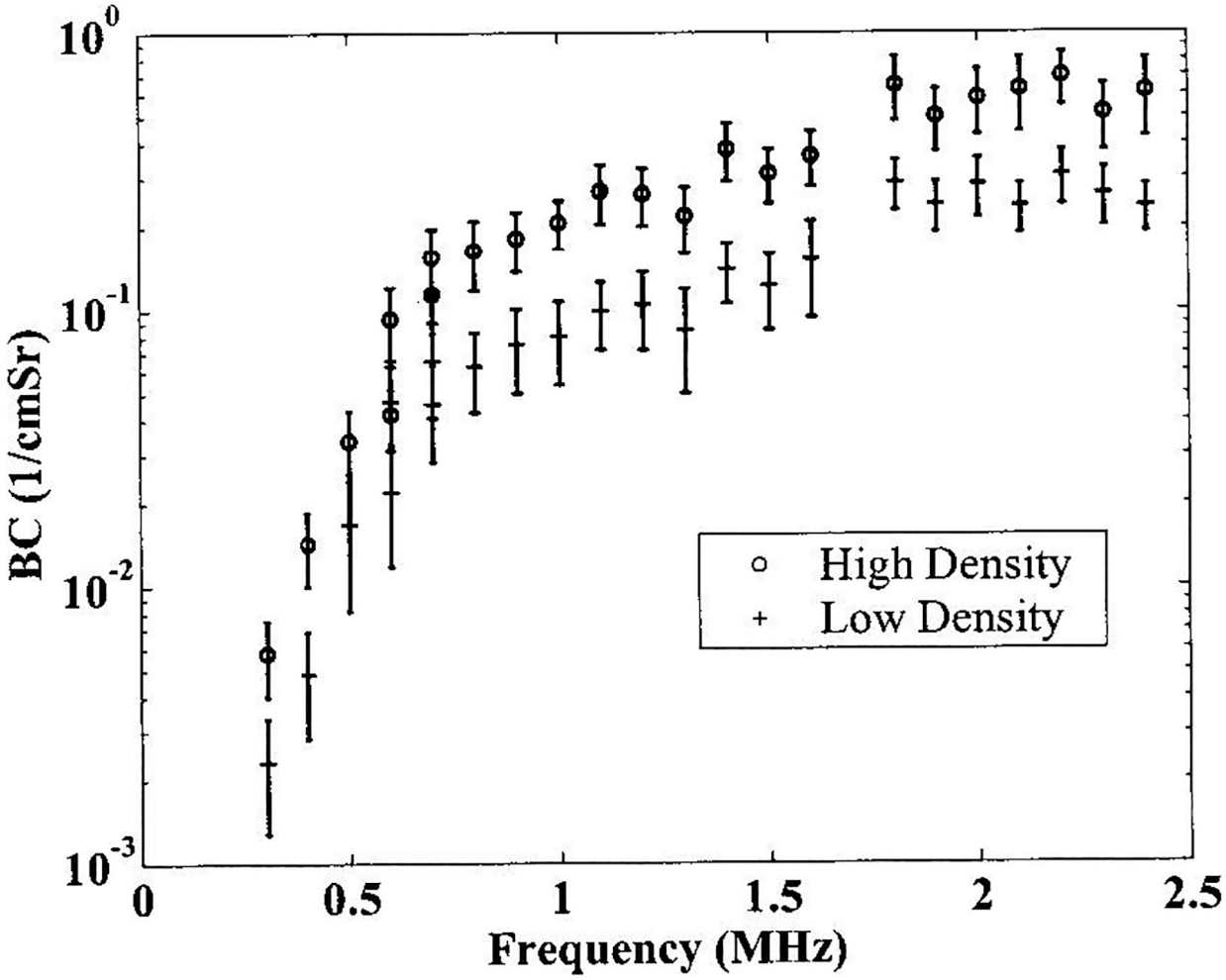

Figure 7.

Frequency dependent experimental measurements for backscatter coefficients for two subgroups of the bone samples: the 8 lowest density (circle) and the 8 highest density (+). Both subgroups exhibit essentially the same frequency dependence. The high-density group backscatters more strongly in a uniform fashion throughout the set of frequencies employed. Error bars denote standard errors of measurements.